

Microwave system for ^{85}Rb and ^{87}Rb hyperfine transitions and Feshbach resonances

Théo Rybarczyk

QDG laboratory

University of British Columbia



Contents

I	Microwave system for ^{85}Rb and ^{87}Rb hyperfine transitions	2
1	Frequency multiplication and stabilization	4
1.1	Phase locked loop	4
1.1.1	About the loop	4
1.1.2	PLL stability	7
1.1.3	Oscillations in VCO input signal	7
1.1.4	Frequency stability of different reference signals	9
1.2	Reaching 3.0 GHz and 6.8 GHz	13
2	Power amplification and stabilization	16
2.1	Power amplification	16
2.2	Power loop	16
3	System behavior	20
3.1	Temperature sensitivity of RF components	20
3.2	RbSS switch on time	21
3.3	Output power as a function of setpoint voltage	25
4	Helical antennae	27
II	Feshbach resonances	31
5	A glimpse at quantum collision theory	32
5.1	Elastic collisions	32
5.1.1	Asymptotic scattering wave function	32
5.1.2	Partial wave analysis	33
5.1.3	Cold elastic collisions	33
5.1.4	Conclusion	35
5.2	Inelastic collisions	35

5.2.1	Spin exchange collisions	35
5.2.2	Magnetic dipole relaxation	36
5.2.3	Three bodies molecular recombination	36
6	Feshbach resonances	37
6.1	Introducing Feshbach resonances	37
6.2	Trap life time applying an homogeneous magnetic field	38
6.3	Searching for Feshbach resonances	41

Part I

Microwave system for ^{85}Rb and ^{87}Rb hyperfine transitions

Overview

The purpose of this system originally designed by Alan Robinson [1] is to deliver, respectively for ^{85}Rb and ^{87}Rb , 3.0 GHz and 6.8 GHz signals (possibly simultaneously) at a maximum power of 1 W from 75 MHz and 85 MHz reference signals to promote electrons from the lower hyperfine state of the $5S_{1/2}$ level to the upper one (see fig. 1, data from [2]).

The first stage is to multiply these reference frequencies by 10 using a phase locked loop (PLL) controlling the output frequency of a voltage controlled oscillator (VCO). Then the VCO output is passed through frequency doublers, band pass filters and amplifiers so that harmonics are damped. In the end the microwaves are amplified up to almost 1 W, this output power is controlled with what I will refer to as the "setpoint" voltage. Furthermore the final power of both signals are stabilized by another loop ("power loop"). The principles and function of each stage and the problems I encountered while constructing them will be explained in detail in the different sections of this report.

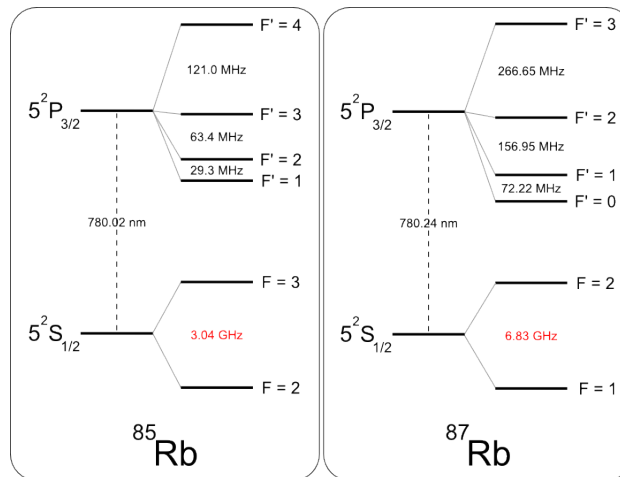


Figure 1: ^{85}Rb and ^{87}Rb energy levels

Chapter 1

Frequency multiplication and stabilization

1.1 Phase locked loop

1.1.1 About the loop

The VCO is used to produce the ten times greater frequency signal. Its output frequency, f_{VCO} , is controlled via a DC signal. A PLL is used to lock this frequency onto the reference, you can find the diagram of the loop in figure 1.1. For more details on PLLs including mathematical description see ref. [3].

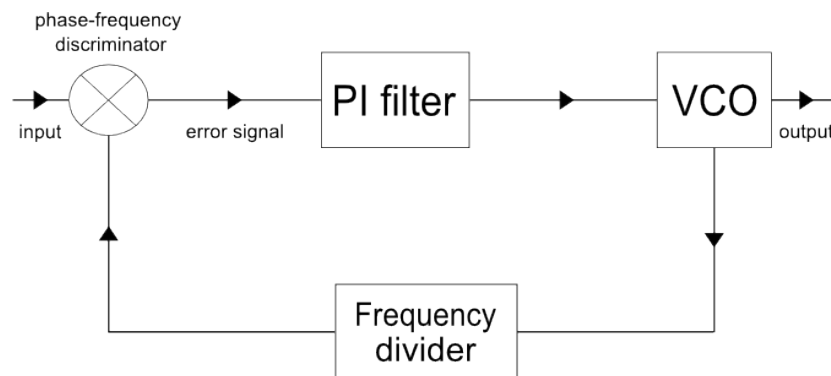


Figure 1.1: PLL diagram

The reference signal (of frequency f_{ref}) and the VCO phases are compared with a UBC made phase/frequency discriminator based on a Analog Device AD9901 chip. If the frequencies of the two signals are not close enough the device will switch to frequency comparison. In both cases it will create a DC

signal ("servo" signal) which is proportional to the phase difference between the VCO output and the reference signal.

It is necessary to include a filter to cut the high frequencies. The main feature of this filter is two proportional integrative (PI) amplifiers. A voltage rectifier is used to cut all negative voltages since the VCO only withstands positive ones. For the filter schematics please refer to fig. 1.3, pictures of the boards are shown fig. 1.2.

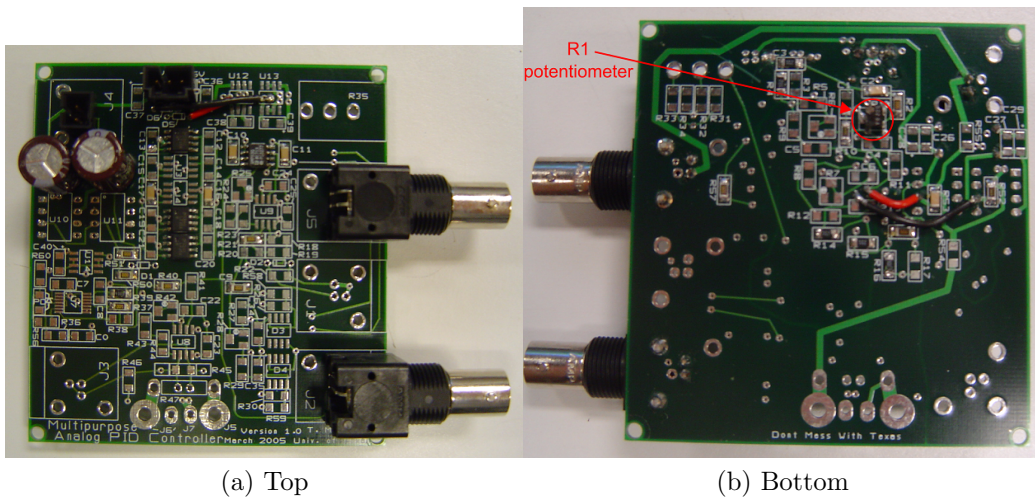


Figure 1.2: Pictures of the PLL filter

Since we want the VCO to produce higher frequencies, its coupled output frequency is divided by $2N$ (N can be set on the PLL box front panel) so that if the loop is locked $f_{VCO} = 2Nf_{ref}$. N is set to 5 for both lines. After the VCO, each signal goes through a certain number of frequency doublers (see Chapter 2). Table 1.1 sums up the different frequency multiplications.

goal	reference	VCO output	number of doublers
3.0 GHz	75 MHz	750 MHz	2
6.8 GHz	85 MHz	850 MHz	3

Table 1.1: Getting the wanted frequencies

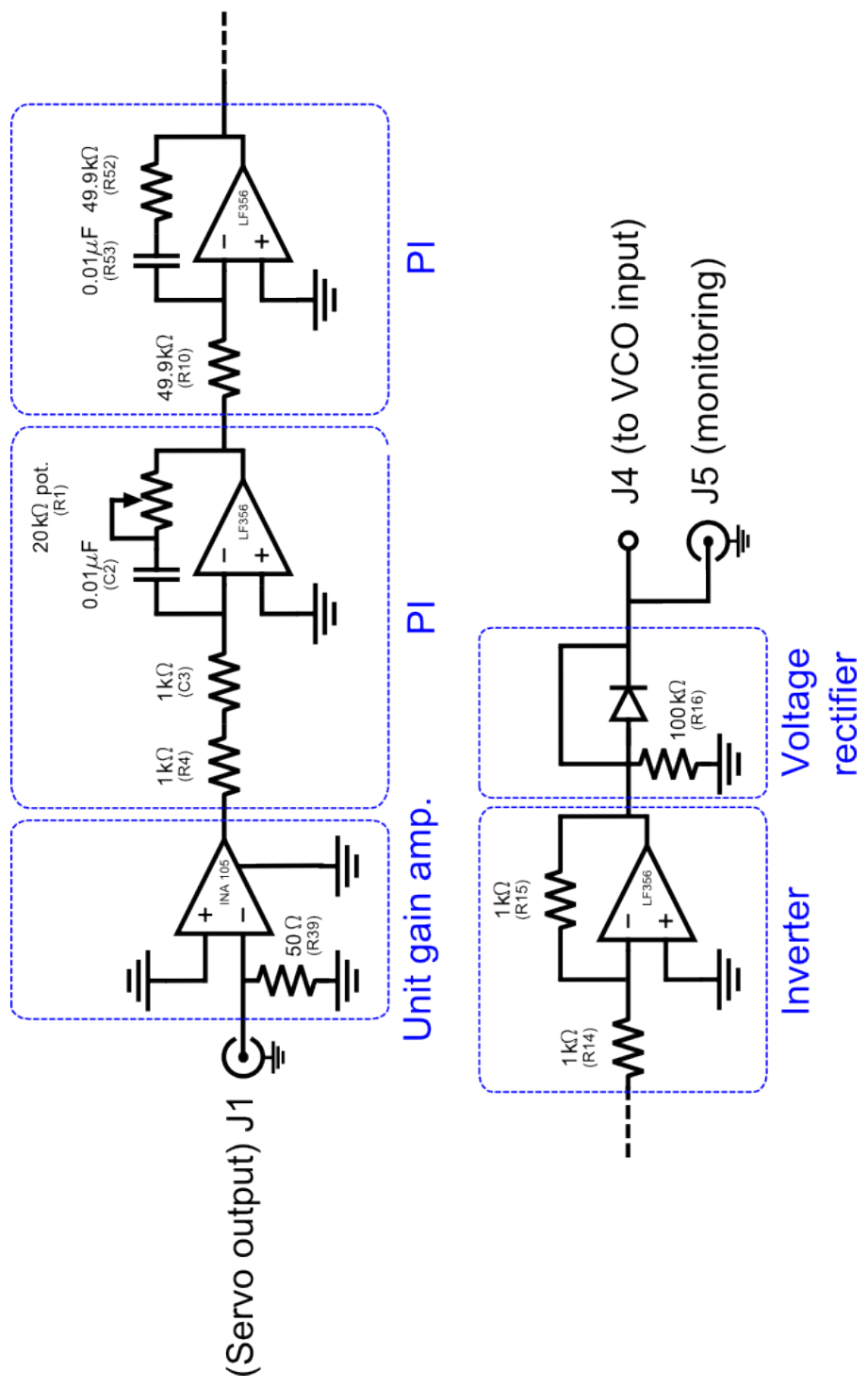


Figure 1.3: PLL filter schematic

frequency	servo gain	R1 (Ω)	τ (μs)
3.0 GHz	1.53	625	20 ± 1
6.8 GHz	1.53	498	17 ± 1

Table 1.2: PLL parameters values and stabilization time

1.1.2 PLL stability

If the loop is locked it also has to be stable. To ensure this I applied a 100 kHz step to the frequency reference to see the loop response. To produce the reference signal I used an Agilent 8648A function generator and the frequency was shifted by applying a square wave to the FM MOD input. This square wave was produced by a Stanford Research System DS345 function generator. For the test of the 3.0 GHz VCO and servo, the reference was changed from 75.0 MHz to 75.1 MHz resulting in a shift of the VCO frequency from 750 MHz to 751MHz. This means that the servo signal (proportional to the phase difference of VCO and reference signals) will suddenly change and because of the loop inertia it will take some time before reaching the steady state. One must adjust some loop parameters to avoid oscillations and to minimize the stabilization time.

Two parameters are adjustable, they are the servo gain (which is a proportional gain: increasing it means having a faster response but also risking to make the loop unstable) and the R1 potentiometer (which controls the ratio of proportional gain over integrative time constant for the first PI filter within the PLL filter: favoring the integrative component over the proportional one results in better stability but increased transient regime duration). The loop responses for both lines are shown in figures 1.4 and 1.5, the time τ it takes for the loop to stabilize and the chosen parameters values are given in table 1.2

1.1.3 Oscillations in VCO input signal

The first time I tried to measure the stability of the PLL applying a 100 kHz step to the reference frequency, I could see that the expected response curves were there but a 11 MHz oscillation with large amplitude was added to it. Note that the loop was still locked despite the oscillations, which means the VCO does not respond to such frequencies.

I could see this effect on both PID controllers (PLL filters) so it was probably not a board defect. After probing the entire board I found that

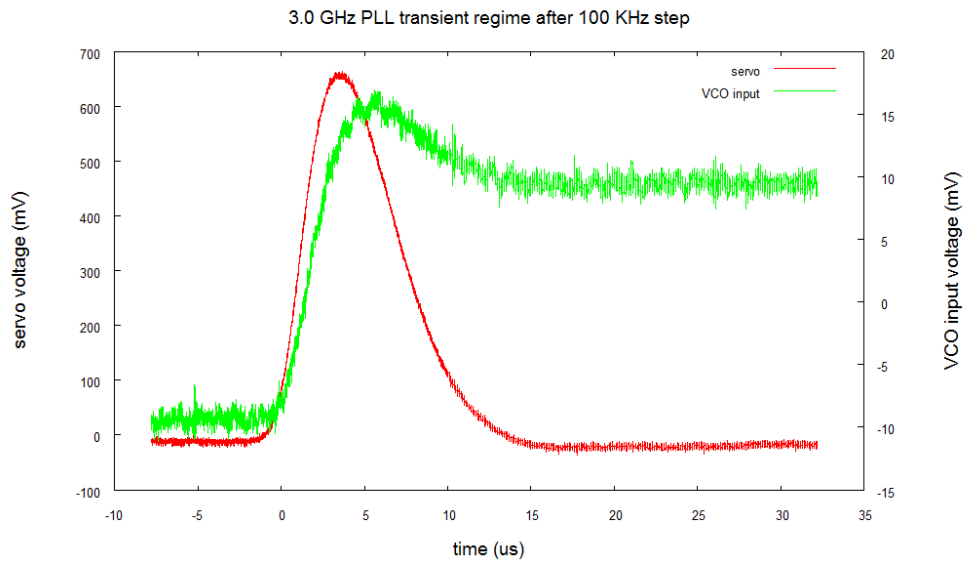


Figure 1.4: Transient regime while applying a 100 kHz step to the reference frequency - 3.0 GHz line

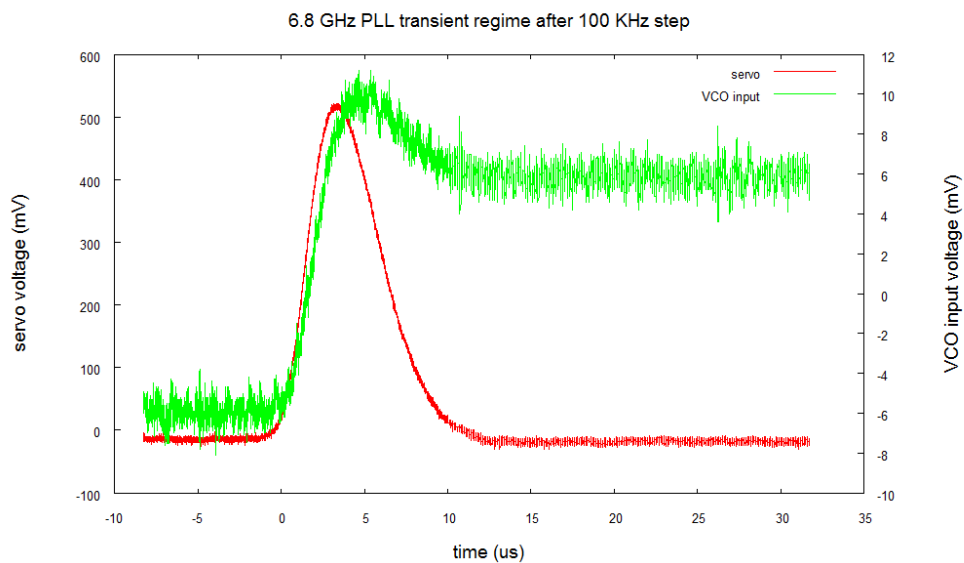


Figure 1.5: Transient regime while applying a 100 kHz step to the reference frequency - 6.8 GHz line

when I touched the V_- input of the inverter op-amp the oscillations were removed. It was because the probe filtered away this frequency component. I did not want to add a new filter to the PID controller since it would have

change the behavior of the PLL. After some investigation I found that the op-amps used for the RbSS I worked on were not the same as in the first RbSS system. I used some OP37G and the first RbSS used LF356 op-amps, so I replaced them all. This simple change removed completely the oscillations. It appeared that the LF356 has a 5 MHz gain-bandwidth product and the OP37G has one of 50 MHz. Using the LF356 which has a lower gain-bandwidth product produced a servo signal without the 11 MHz oscillations.

1.1.4 Frequency stability of different reference signals

The RbSS reference oscillation will be produced by DDSs (Direct Digital Synthesizers) but for my tests during the set up of the system I used the Agilent 8648. When I tried to use a DDS as reference I saw "dirty" transient curves (servo and VCO input) when applying a frequency step to the DDS (see figures 1.6 and 1.7 and compare with figures 1.4 and 1.5)

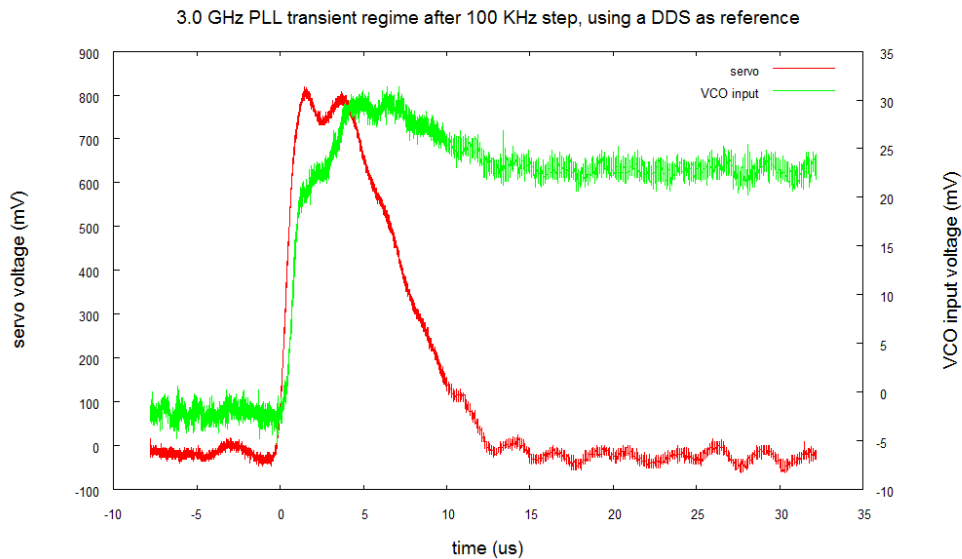


Figure 1.6: Transient regime while applying a 100kHz step to the reference frequency from a DDS - 3.0 GHz line

The DDS set at 75 MHz or at 85 MHz is actually locked onto a first DDS set at 15 MHz locked itself onto the master clock. Thus I took some spectra of the three sources: the Agilent, the DDS set at 75 MHz and the output of the first DDS at 15 MHz. The spectra are shown in figure 1.8 with a zoom into a narrower range around 75 MHz in figure 1.9. On both graphs the DDS

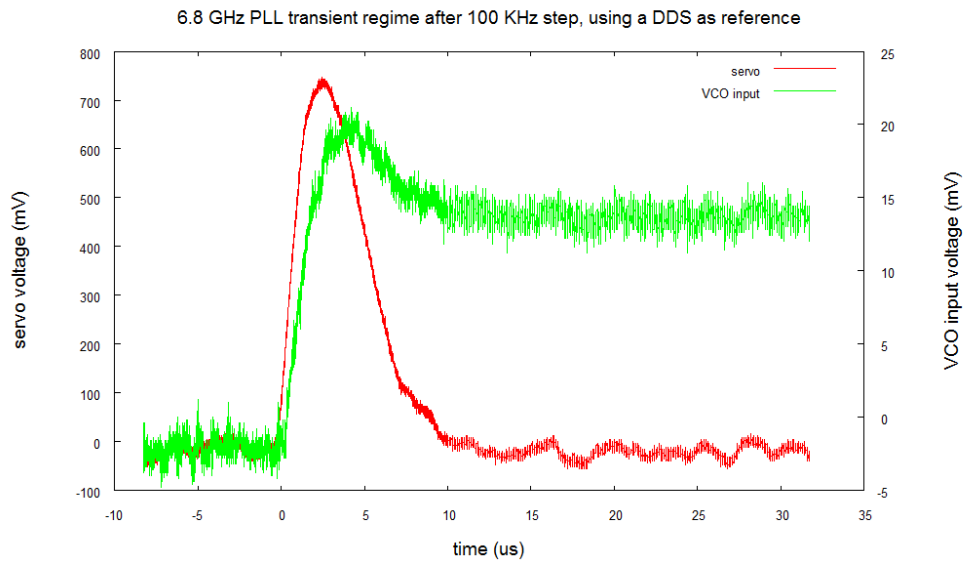


Figure 1.7: Transient regime while applying a 100kHz step to the reference frequency from a DDS - 6.8 GHz line

at 15 MHz is centered at 75 MHz for an easier comparison with the other two curves.

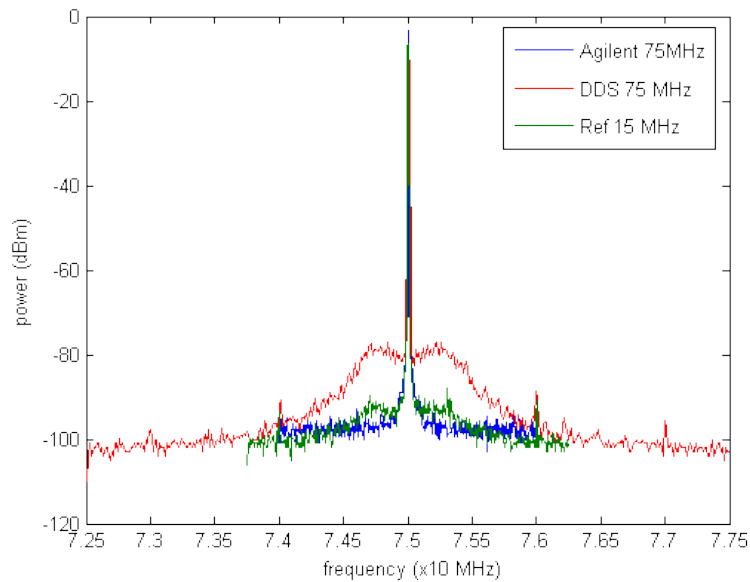


Figure 1.8: Reference signals spectra

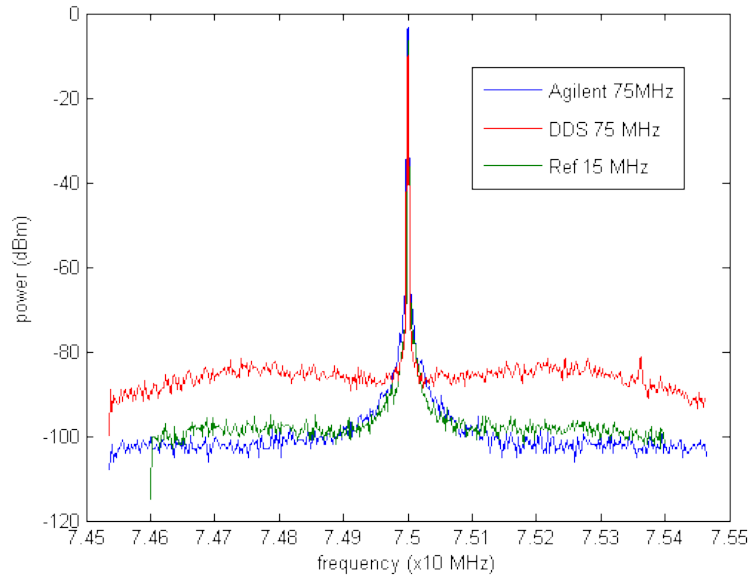


Figure 1.9: Close-up

There is an evident difference in linewidth, the Agilent has obviously a better frequency stability. Wings to the central DDS at 75MHz peak are about ten times larger than the Agilent peak. This is most certainly an effect of the PLLs used in the DDSs to multiply the frequency of a source. Since the DDS at 75 MHz is locked on to the DDS at 15 MHz, it means two PLLs are needed to produce the desired signal. If each PLL has phase noise it is natural that the output has frequency noise which is amplified if several PLLs are used.

Though these wings are at quite low power relative to the peak power, it has effect on the 750 MHz spectra taken at the VCO coupled output as shown in figure 1.10. Increasing zooms are shown in fig. 1.11 and 1.12. Of course when using the 15 MHz DDS as the reference for the RbSS, N has to be set to 25.

It may not be a problem of great importance but this is yet to be confirmed using this second RbSS in the experiment.

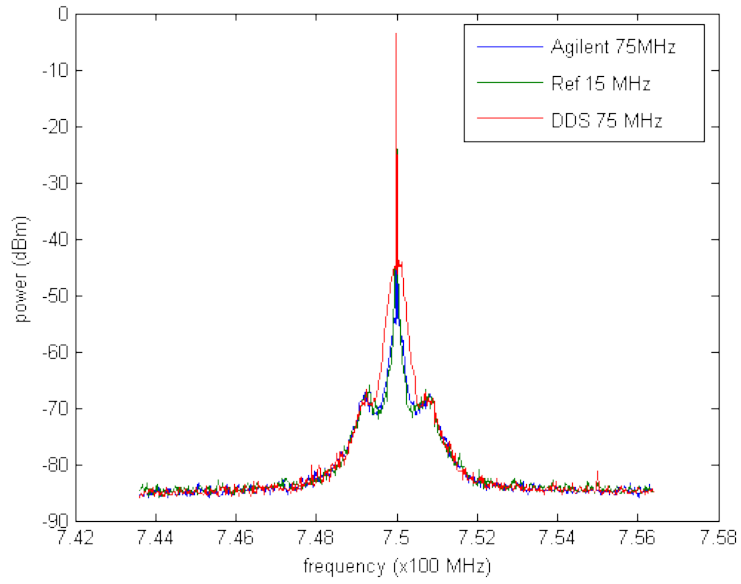


Figure 1.10: VCO output spectra for the three sources

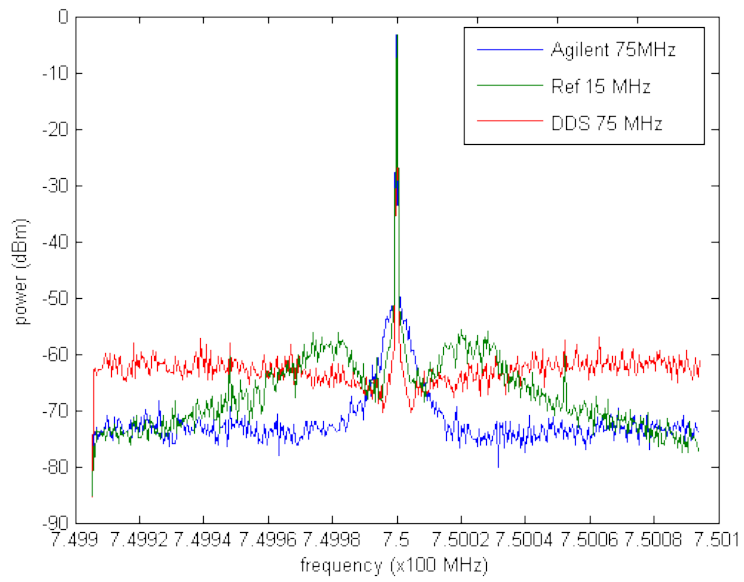


Figure 1.11: Zoom 1

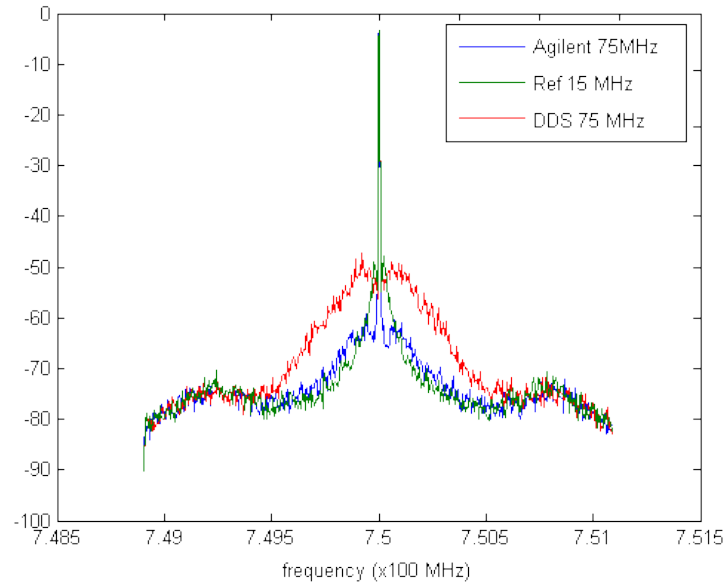


Figure 1.12: Zoom 2

1.2 Reaching 3.0 GHz and 6.8 GHz

As said in the overview, before amplifying the signals it is necessary to have the wanted frequencies with harmonics from the VCO output damped to the maximum. That is why after each frequency doubling, the signals are band-pass filtered then amplified to maintain a certain power level. In figures 1.13 and 1.14 you can see a block diagram (of the first box) showing the frequency multiplication stage and the power loop filter for both frequencies.

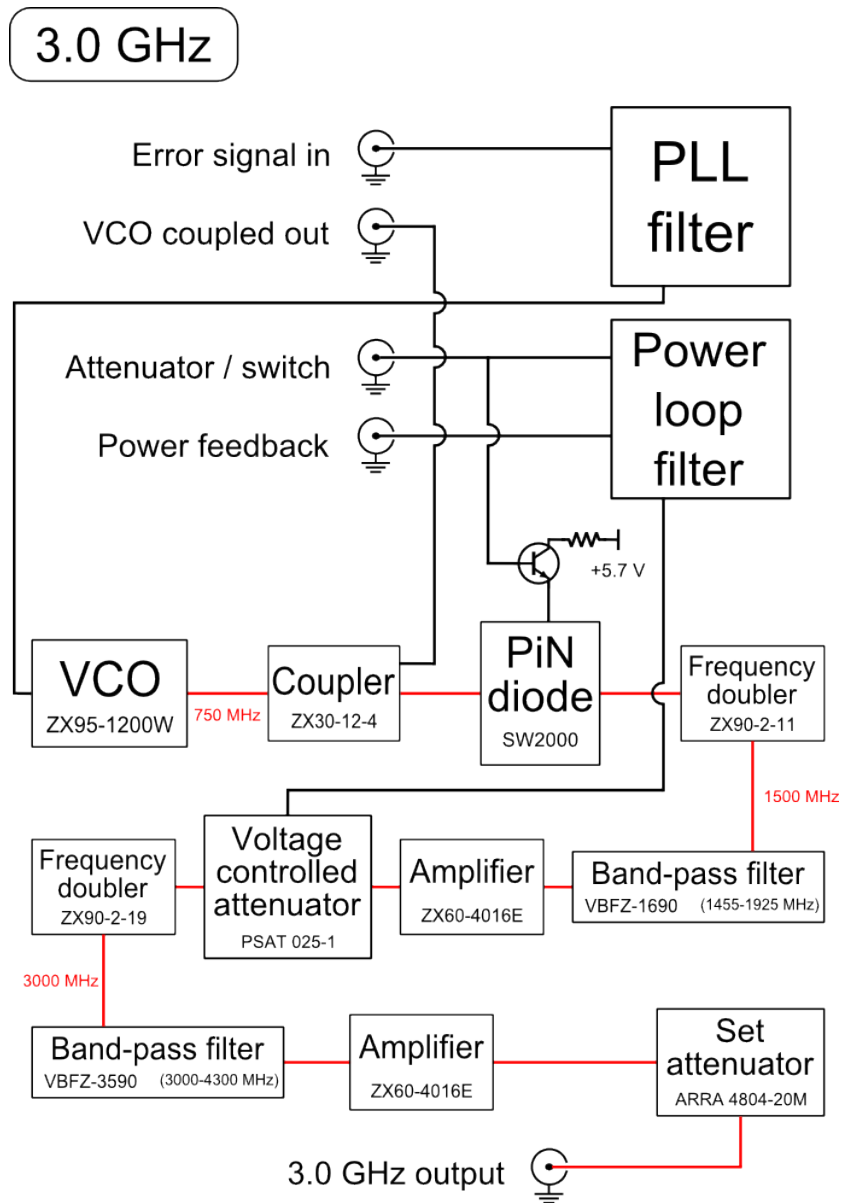


Figure 1.13: Block diagram of the first box : frequency multiplication and power loop filter

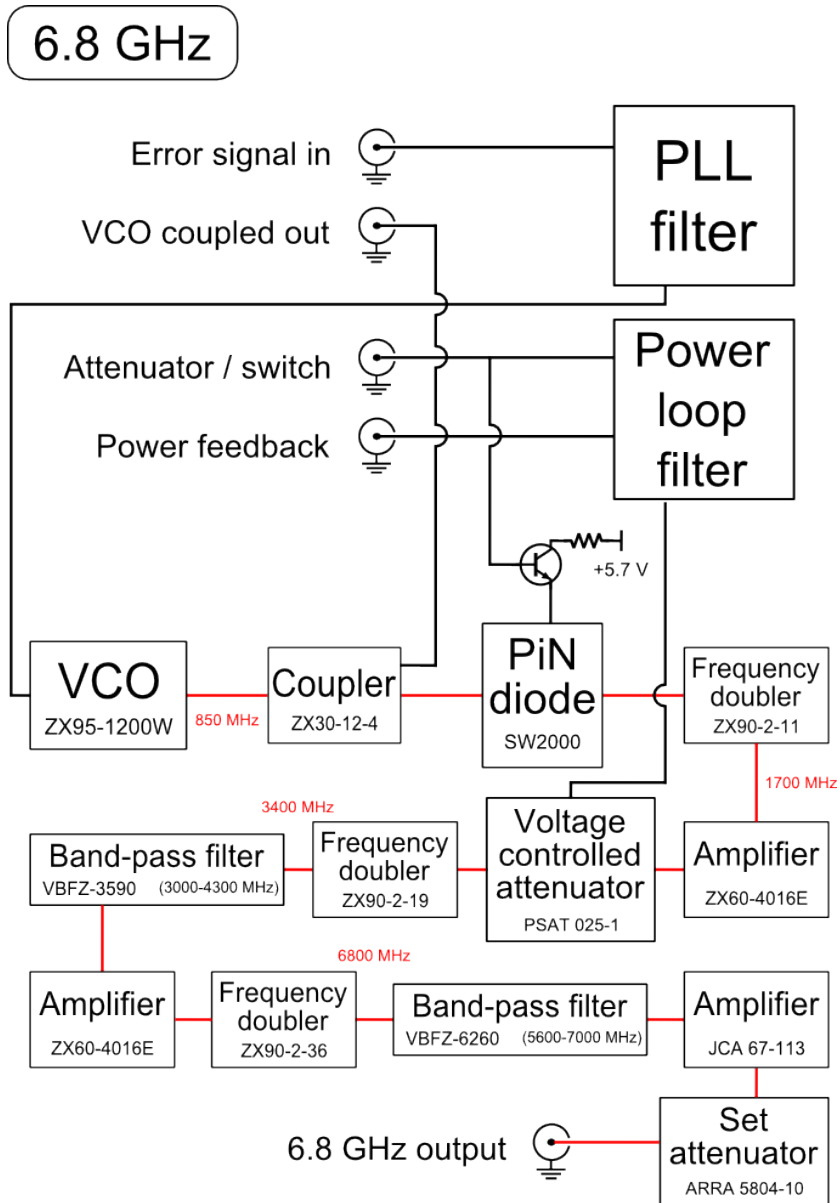


Figure 1.14: Block diagram of the first box : frequency multiplication and power loop filter

Chapter 2

Power amplification and stabilization

2.1 Power amplification

The output from the first box is sent to a second box ("power box") which contains the last amplifiers to reach approximately 1 W. The block diagram is shown fig. 2.1. Each line has one or two amplifiers, the amplified signal go through a 20 dB coupler, most of the power goes to the reed (mechanical) switch and then to the output. The 20 dB coupled output is for the power detector which can not bear power higher than 20 dBm. There are also isolators so that, when the reed switches are opened, the power is dissipated in them and does not come back through the previous RF components.

2.2 Power loop

As said previously, the output power of the RbSS system is also stabilized with a loop. We set the desired power with the "setpoint" DC voltage from an analog output controlled via a python program. The setpoint is compared with the DC voltage coming from the power detector. This difference signal is produced on the power loop filter which is in the first box as seen in figures 1.13 and 1.14. This signal, after passing through filters, is sent to a VCA (voltage controlled attenuator) which is also in the first box. The VCA has a logarithmic relation between its DC input and how it attenuates the RF signal, so there is also an exponential amplifier on the power loop PID controller to make the relation between the setpoint and the actual attenuation as linear as possible. Please note that the setpoint voltage is

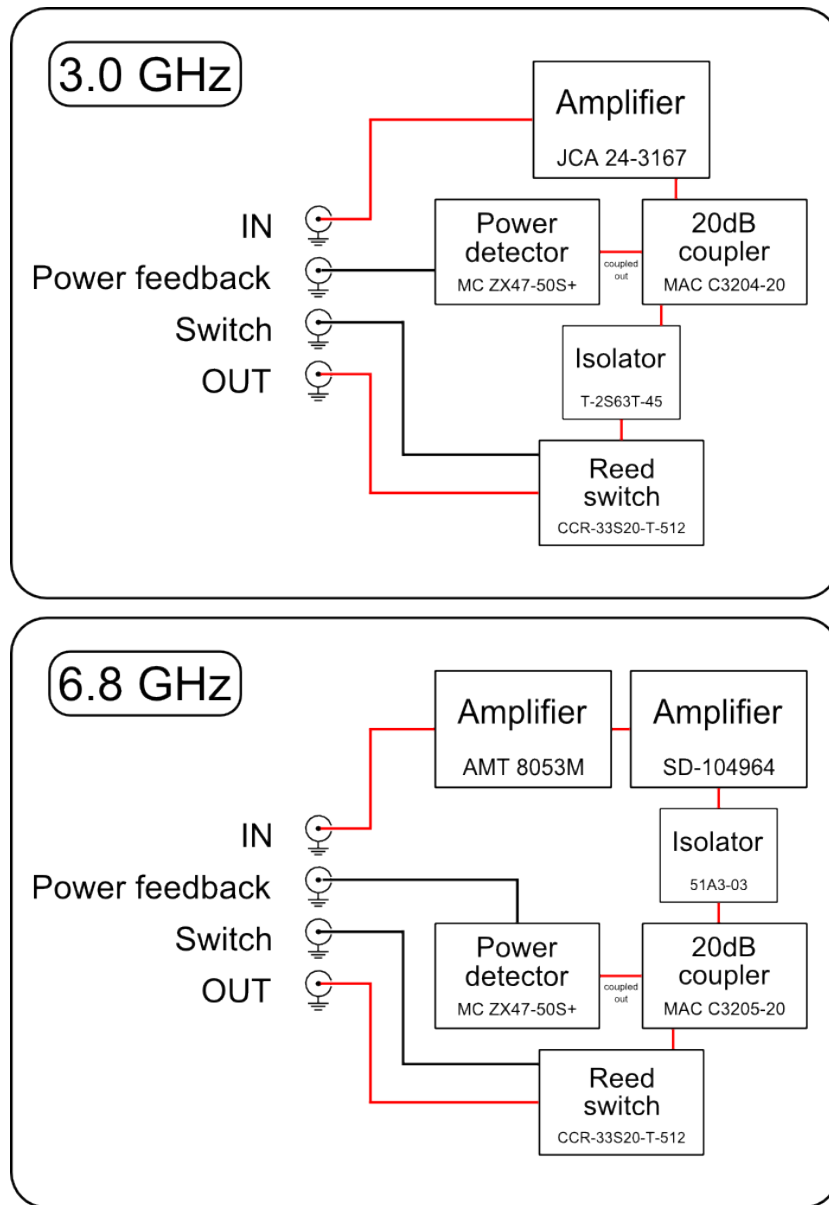


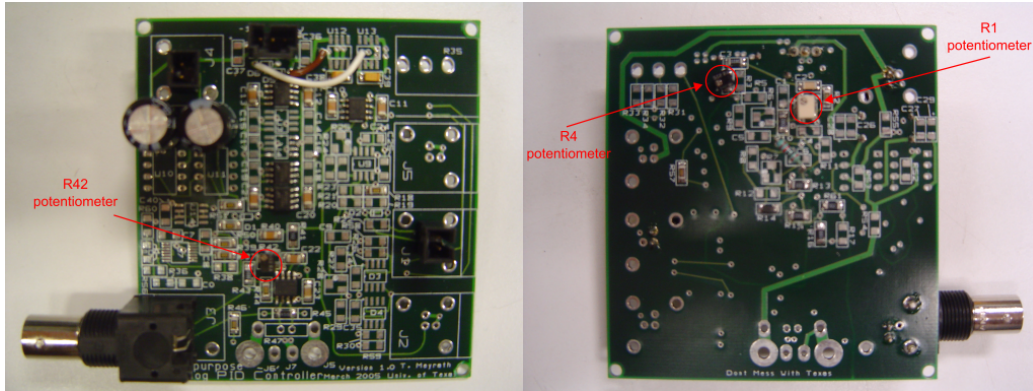
Figure 2.1: Block diagram of the second box : power amplification and stabilization

also sent to a MOSFET controlling a PiN diode (see figs. 1.13 and 1.14), thus the diode is used as an early switch which is open for 0 setpoint. The power loop filter schematic is shown fig. 2.3, pictures in fig. 2.2. The INA 154 amplifier outputs the difference between the setpoint voltage and the power detector output. As the diode is not completely on before a 4 V setpoint,

the larger setpoint range has to be from 4 V to 10 V. The power detector approximately outputs from 0.6 V to 2 V, it is thus necessary to multiply the power detector output so that we can use the wider range of setpoint possible. There is a INA 128 amplifier which gain is tunable and given by $G = 1 + \frac{50 k\Omega}{R42+R43}$ with $R43 = 3.83 k\Omega$, with notation consistent with the schematic fig. 2.3. This filter has adjustable parameters controlled by three potentiometers. Optimal values as well as the INA 128 gain can be found in table 2.1. R1 controls the integrative time constant and proportional gain for the PI filter and R4 acts only on its proportional gain. R42 controls the gain of the INA 128 amplifier.

frequency	R42	R4	R1	calculated INA 128 gain
3.0 GHz	3.48k Ω	2.84k Ω	16.7k Ω	7.83
6.8 GHz	4.79k Ω	2.79k Ω	16.5k Ω	6.80

Table 2.1: PLL parameters values



(a) Top

(b) Bottom

Figure 2.2: Pictures of the power loop filter

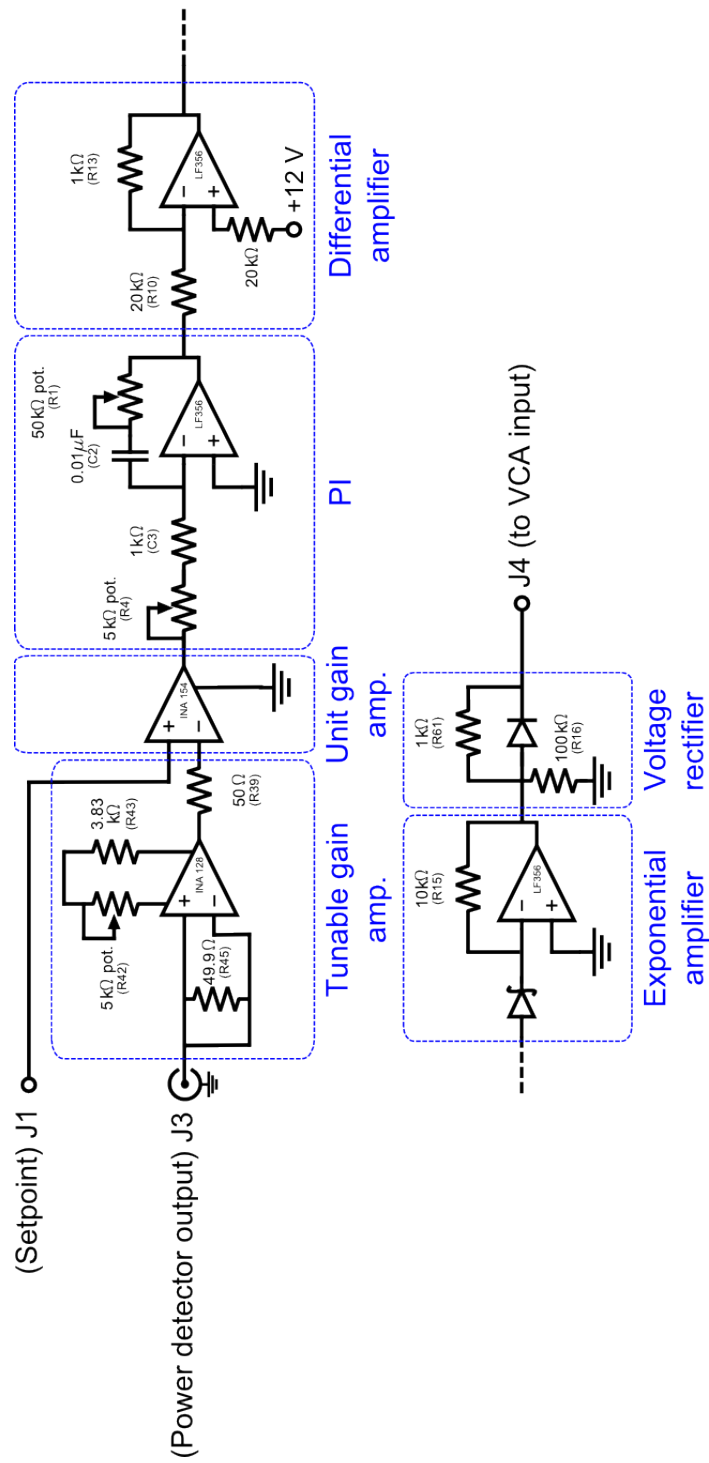


Figure 2.3: Power loop filter

Chapter 3

System behavior

3.1 Temperature sensitivity of RF components

When I tried to measure the output power versus setpoint I realized that the maximum power varied with time. It appeared that is was also the case for lower powers and that the most probable reason to this effect was that at least one component (amplifier, power detector...) was temperature sensitive. This is a rather small effect so it certainly won't be a problem for microwave transitions since the maximum power fluctuations are about 0.5 dBm. The power variation time was difficult to evaluate. To have a rough idea about it, I measured the output power two different ways with a spectrum analyzer. One way ("fast" way) was to let the signal out for a time no longer that what it takes for the spectrum analyzer to average (over 30 spectra), that is about 15 s, then shut down with 0 setpoint and wait about 30 s to let the system cool down and then repeat the procedure over a large power range. The second way ("slow" way) was to set the power and then wait 30 mn before taking the data point. The results are shown fig 3.1 and as you can see, the difference is far from huge on this particular measurement. The only thing I can conclude is that the power varies over minutes (or dozens of seconds), but I don't have precise variation times.

I attempted to know which component(s) was (were) temperature sensitive, blowing hot air with the heat gun on different spots. I saw a drop of power for the 3.0 GHz line but nothing for the 6.8 GHz. The reason why this test was inconclusive was that I could not be sure which component I hit with the heat gun since the area covered was too large. The power drop could be a result of melting solder of some electronics leading to a malfunction of the amplification. I stopped the test by fear of damaging a component as some

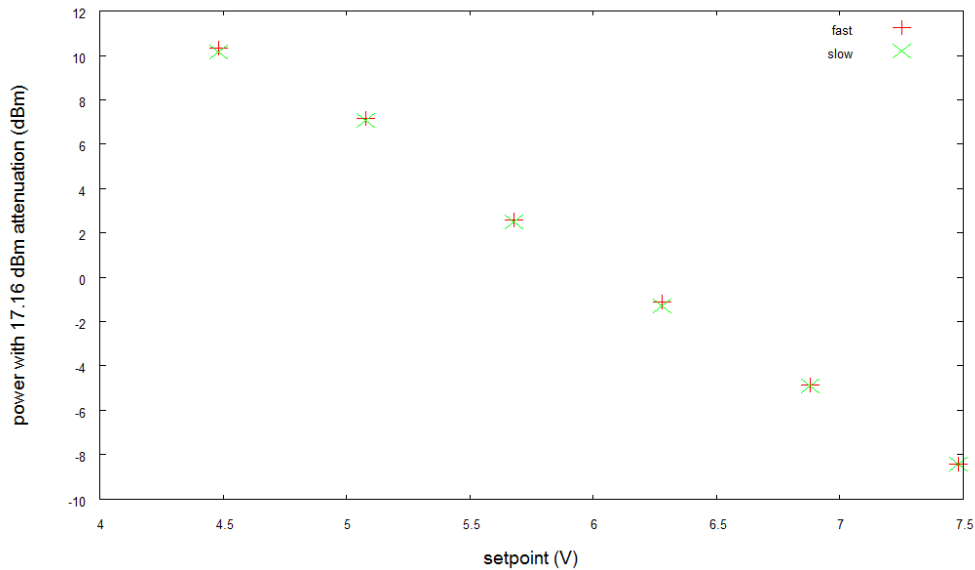


Figure 3.1: Power variation with time because of temperature

wires started to melt.

3.2 RbSS switch on time

How fast is the system to completely turn on (that is delivering a stable 1 W microwave signal) was of the greatest importance. Benjamin Deh reported that the first system was unable to function below ≈ 5.5 ms after turning on. So I measured different switching on times: how fast is the system to be stable with the reed switch closed and how fast is actually this mechanical switch to close.

For the first one I just took the PLL phase monitor signal while going from 0 setpoint to max power setpoint for both 3.0 GHz and 6.8 GHz. The results are shown fig. 3.2 and 3.3. The difference between those one and the PLL transient curves from the PLL stability study is that here we consider the whole system and not only the PLL. Now there is some coupling between frequency multiplication and power stabilization resulting in a longer stabilization time.

To measure the closing time of the reed switches I needed to take the 3.0 GHz and 6.8 GHz output signals. I tried to use a Tektronix 11801B oscilloscope which can go up to 50 GHz but I could not figure out how to trigger it, which is somehow frustrating since it is a digital oscilloscope. So I ended us-

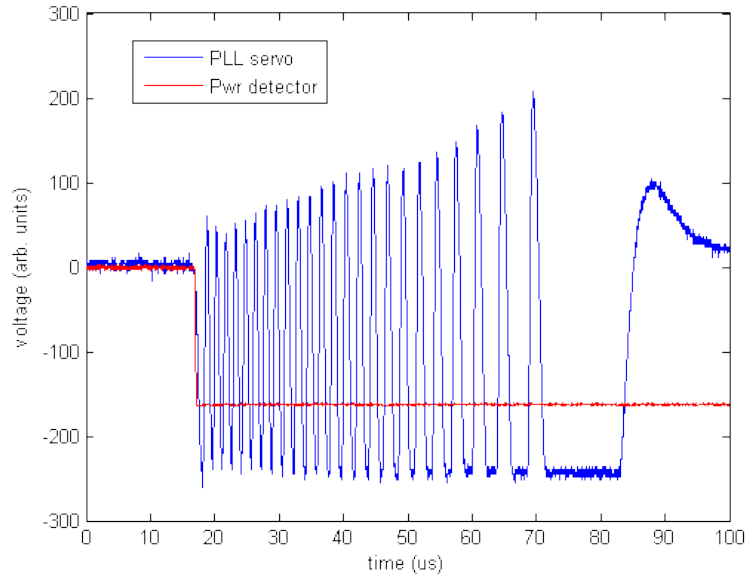


Figure 3.2: Stabilization of 3.0GHz signal - $(85 \pm 1)\mu s$

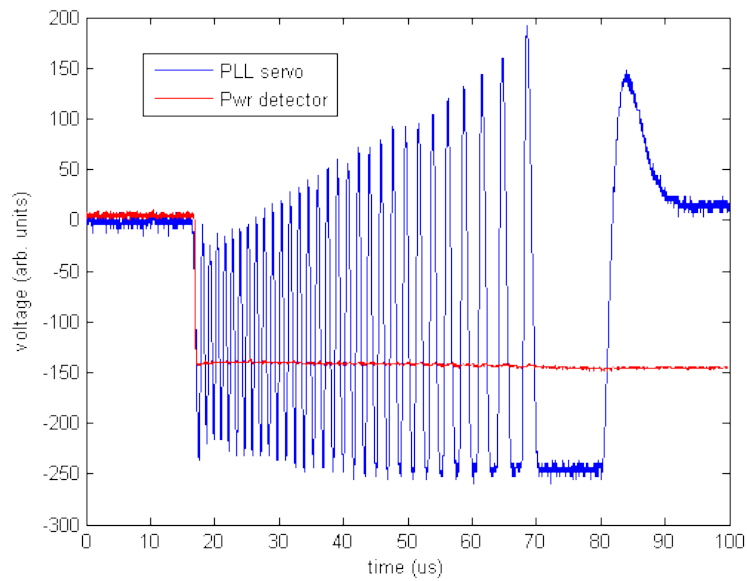


Figure 3.3: Stabilization of 6.8GHz signal - $(79 \pm 1)\mu s$

ing a Tektronix TDS 3014 and even though it can't trace these frequencies I could see something. You can see the time it takes for the mechanical switch to close in figures 3.4 and 3.5, note the bouncing. The times I measured are

consistent with the observation of B. Deh.

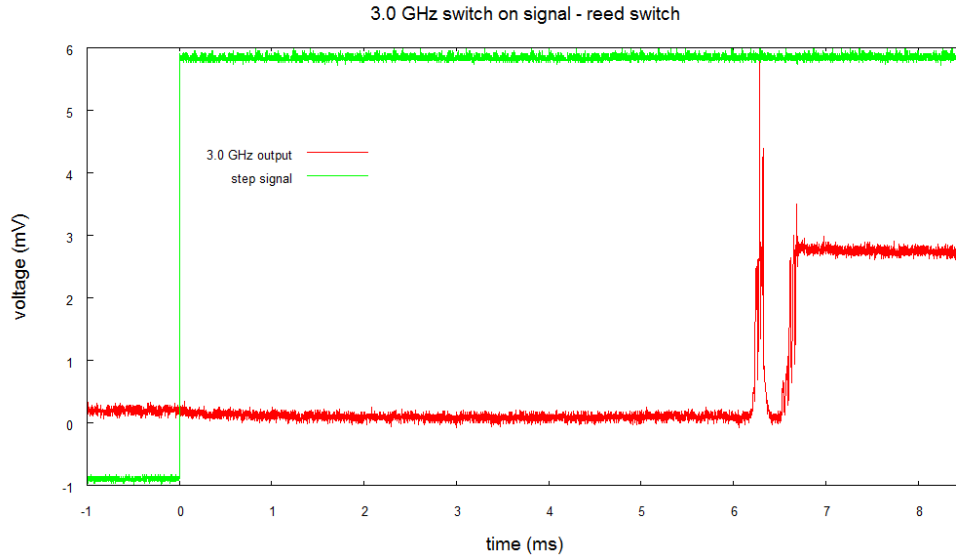


Figure 3.4: 3.0GHz - Reed switch closing time : $(6.7 \pm 0.1)ms$

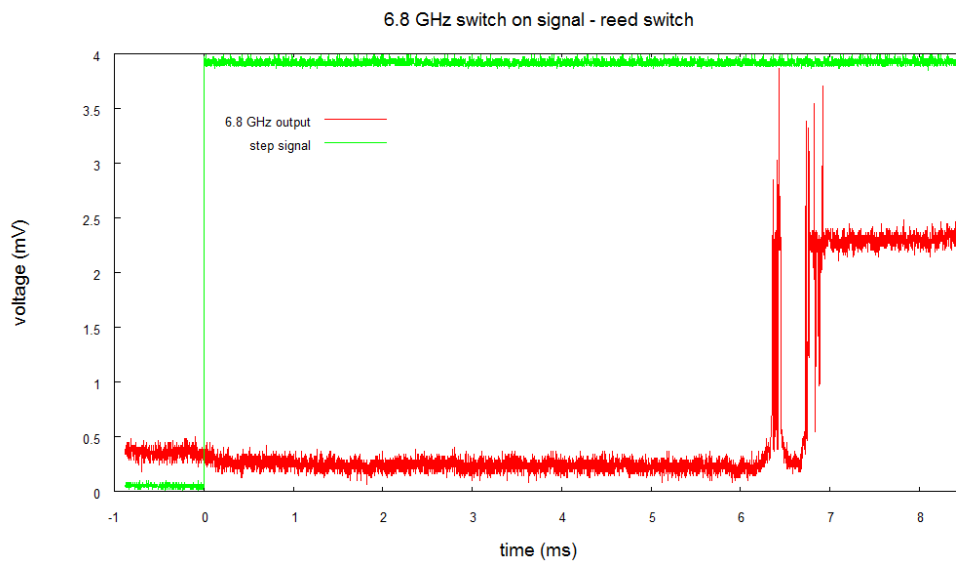


Figure 3.5: 6.8 GHz - Reed switch closing time : $(7.0 \pm 0.1)ms$

Using the same method I measured again how long it takes for the system to stabilized while applying a setpoint step. I found similar times to those I

found monitoring the servo signal as shown in figures 3.6 and 3.7.

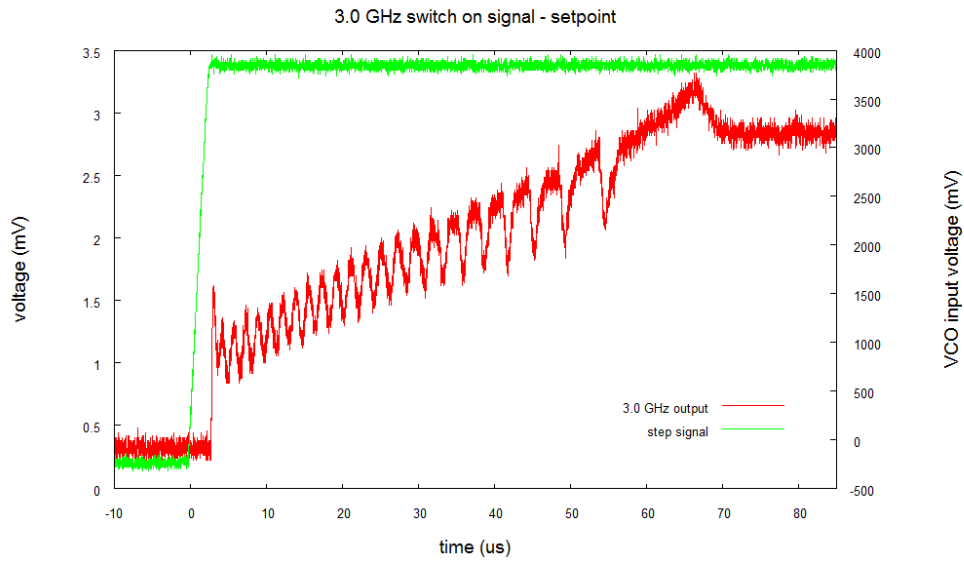


Figure 3.6: Stabilization of 3.0GHz signal - $(73 \pm 2)\mu s$

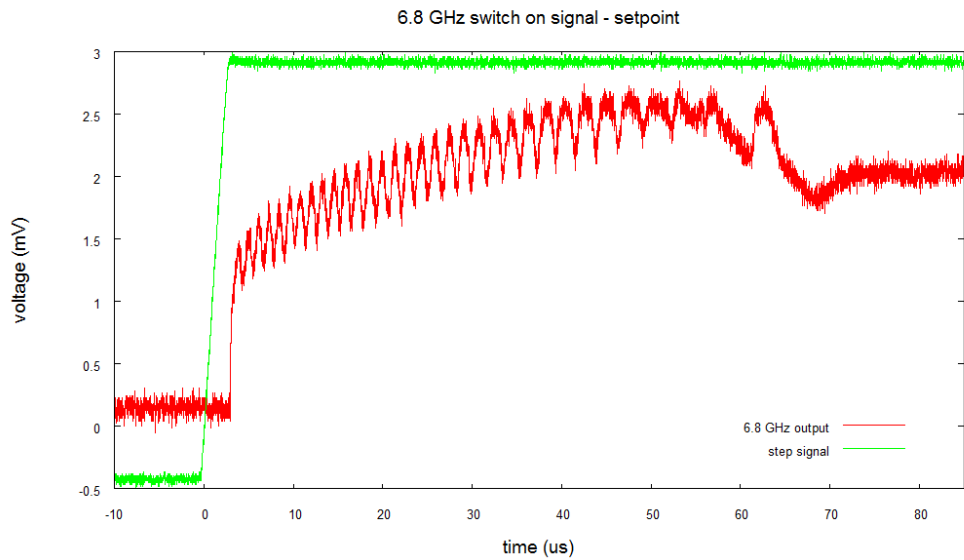


Figure 3.7: Stabilization of 6.8GHz signal - $(74 \pm 2)\mu s$

These results will be helpful to write a good code sequence and thus be able to use the system for time inferior to the millisecond.

3.3 Output power as a function of setpoint voltage

To measure the output power I used a spectrum analyzer with an average over 40 spectrum. I let the microwaves out for 10 s for each data point with a waiting time superior to 10 s between two measurements to avoid temperature effects. The curves with fits are shown figures 3.8 and 3.9.

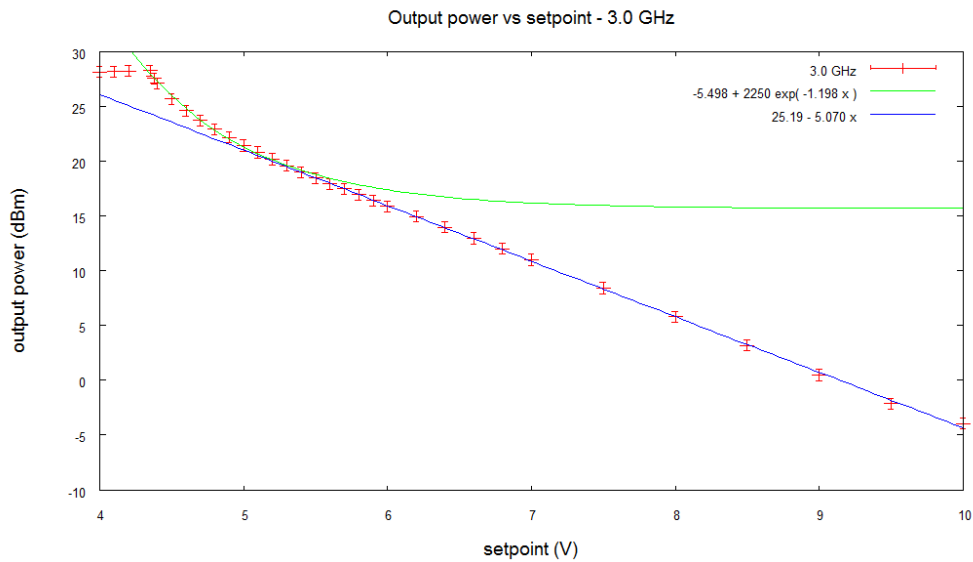


Figure 3.8: Output power versus setpoint - 3.0 GHz

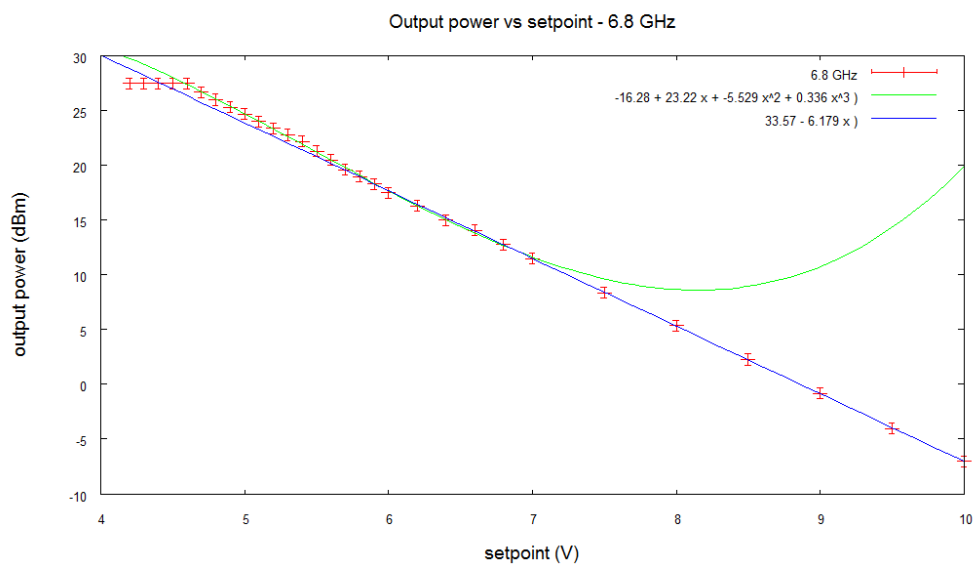


Figure 3.9: Output power versus setpoint - 6.8 GHz

Chapter 4

Helical antennae

Currently, the antennae used are $\lambda/2$ dipole antennae. They are simple and efficient antennae but they have low directivity: they emit in a quite big solid angle even with the help of reflectors. A more directive antenna and not so complicated to make is the helical antenna. It is characterized by three parameters, its diameter D (or identically, its circumference C), the helix pitch angle α and the number of turns N (see fig 4.1). Another quantity has to be introduced which is the spacing between two turns S . Length quantities expressed in units of the radiation wavelength in the antenna have a λ subscript.

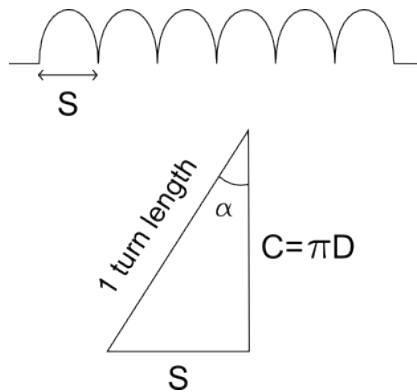


Figure 4.1: Helix geometry

We want the helix to radiate mainly in the direction of its axis (not radially), using ref. [4] we know that to achieve such axial mode, C_λ , α and N must lie within certain ranges which are :

$$3/4 < C_\lambda < 4/3$$

$$12 < \alpha < 14$$

$$N > 3$$

$C_\lambda = 1.20$, $\alpha = 13.0$ and $N = 8$ were used, resulting in $S_\lambda = 0.277$. According to the Kraus' antenna gain formula $G = 11.8 + 10 \log(NC_\lambda^2 S_\lambda)$, these parameters are quite optimal: they allow high gain and axial mode radiation. Trying to get a higher gain involves having C_λ and α too close to their maximum value risking a bad far field radiation pattern. Increasing N will result in a higher gain and a higher directivity but also in a longer helix which is a great issue, so $N = 8$ is a good compromise.

The antenna length has been indeed a severe strain. The 3.0 GHz antenna (just a helical wire) length is $NS_\lambda\lambda_0 = 22.2$ cm (λ_0 being the wavelength in vacuum) which is too long. Antennae should not be longer than 10 cm to fit on the table. The solution is to wind the wire around a dielectric material cylinder with high enough dielectric constant ϵ_r to make the wavelength in the antenna smaller. The length is then given by $NS_\lambda\lambda_0/\sqrt{\epsilon_r}$.

Several machinable materials can be used, the best found was Delrin (polymer) or Mykroy/Mycalex (glass bonded mica). Materials, dielectric constant used for calculation and corresponding helix characteristics for both frequencies are shown table 4.1. For most case the exact ϵ_r for 3.0 GHz or 6.8 GHz was not available, that is why assumptions are made. For higher frequencies, the dielectric constant is expected to drop but in a way which greatly depend on the material used.

Material	f (GHz)	ϵ_r	λ (mm)	L (mm)	D (mm)	S (mm)
PMMA	3.0	2.475 @6.8GHz	63.56	140.88	24.28	17.61
	6.8	2.475 @6.8GHz	28.04	62.15	10.71	7.77
Macor	3.0	5.67 @6.8GHz	42.00	93.08	16.04	11.64
	6.8	5.67 @6.8GHz	18.53	41.06	7.08	5.13
Mykroy/Mycalex	3.0	6.79 @3.0GHz	38.38	85.06	14.66	10.63
	6.8	6.79 @6.8GHz	16.93	37.52	6.47	4.69
Delrin	3.0	3.7 @1MHz	51.99	115.22	19.86	14.40
	6.8	3.7 @1MHz	22.94	50.83	8.76	6.35
	6.8	3.5 assump.	23.58	52.27	9.01	6.53

Table 4.1: Dielectric constants and helix characteristics

Another issue is impedance matching. It can be achieved by partly flattening the first 1/4 wire turn of the helix, that is why there is some spacing between the ground plane and the dielectric core. An external tubing has

been made to cover the wired helix. You can see the antenna model in fig. 4.2.

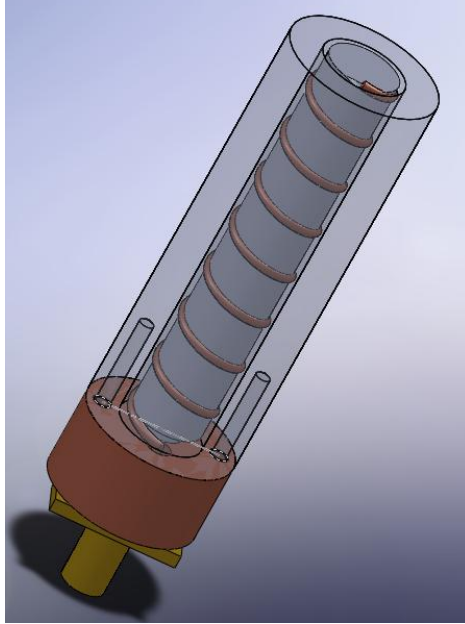


Figure 4.2: Helical antenna designed with Solidworks

A prototype 6.8 GHz antenna was machined using Delrin and assuming $\epsilon_r = 3.5$. Unfortunately the copper base used as a ground plane and a reflector could not have been made on time. A "hand made" squared ground plane with approximately the same dimension was made to replace the missing one. A 0.81 mm diameter copper wire was wound around the Delrin core. This diameter is not a critical parameter since it has to lie between 0.005λ and 0.05λ [4]. A picture of the antenna is shown fig 4.3. Testing this prototype revealed that it was less good than the current 6.8 GHz antenna: for an identical distance to the measurement coil the power was lesser (read with the spectrum analyzer) by several dBm. The reason may be that the dielectric constant assumed was wrong for Delrin at this frequency. A quick directivity test showed that it had side lobes meaning that the antenna was not functioning in pure radial mode. It may also be that the poor manufacture of the ground plane and the lack of precise impedance matching caused a bad field pattern.



Figure 4.3: Prototype helical antenna

Part II

Feshbach resonances

Chapter 5

A glimpse at quantum collision theory

5.1 Elastic collisions

Elastic collisions are of great importance since they thermalize the atomic cloud. Here is a quick proof of the "harmless" effects of such collisions, for more details you can refer to [5], [6], [7]. There is a wide choice in literature for quantum elastic collisions.

5.1.1 Asymptotic scattering wave function

For a two-body collision we can study separately the motion of the center of mass and the relative motion of the two particles. The motion of the center of mass is one of a free particle so the relative motion of the particles will be studied here and considered as a virtual particle (observed in the center-of-mass frame) of mass μ which is the reduced mass of the colliding particles: $\mu = m_1 m_2 / (m_1 + m_2)$.

Let's assume that the potential V felt by the fictitious particle only depends on r , the relative position of the two particles. The time independent Schrödinger equation to solve is then

$$\left(\frac{\mathbf{p}^2}{2\mu} + V(r) \right) \Psi(\mathbf{r}) = E\Psi(\mathbf{r}) \quad (5.1)$$

We can consider the following asymptotic solution:

$$\Psi(\mathbf{r}) \underset{r \rightarrow \infty}{\approx} e^{ikz} + f(\theta, \phi) \frac{e^{i\mathbf{k}\mathbf{r}}}{r} \quad (5.2)$$

It is a superposition of an incoming plane wave (before scattering) and an outgoing spherical wave (after scattering) valid far away the potential effective area. The outgoing wave has a $f(\theta, \phi)$ factor called the scattering amplitude which depends on $V(r)$. Since the problem has a spherical symmetry f does not depends on ϕ : $f(\theta, \phi) = f(\theta)$.

The collision differential cross section $\sigma(\theta, \phi)$ measure the probability to observe a scattered particle in a unit solid angle in the direction given by (θ, ϕ) , it is thus the ratio of the scattered over incoming current density. For an elastic scattering by a central potential this reduce to:

$$\sigma(\theta, \phi) = \sigma(\theta) = |f(\theta)|^2 \quad (5.3)$$

The total cross section σ_T is simply the sum of $\sigma(\theta)$ over all solid angles.

5.1.2 Partial wave analysis

We can switch to a partial wave basis and look for solutions to 5.1 in the form (spherical symmetry is again used to simplify):

$$\Psi(\mathbf{r}) = \sum_{l=0}^{\infty} C_l R_l(r) P_l(\cos(\theta)) \quad (5.4)$$

where P_l are Legendre polynomials, R_l are radial functions and C_l some constants defined by normalization. Let be $u_l(r) = R_l(r)/r$, u_l functions are solutions of

$$\left(\Delta + k^2 - \frac{l(l+1)}{r^2} - U(r) \right) u_l(r) = 0 \quad (5.5)$$

where $U(r) = \frac{\hbar^2}{2\mu} V(r)$. From there we can find the expression of $u_l(r)$ far from the effective range of the potential:

$$u_l(r) \underset{r \rightarrow \infty}{\approx} \sin \left(kr - l\frac{\pi}{2} + \delta_l \right) \quad (5.6)$$

And then we can rewrite f in this new basis:

$$f(\theta) = \sum_{l=0}^{\infty} (2l+1) e^{i\delta_l} \sin(\delta_l) P_l(\cos(\theta)) \quad (5.7)$$

5.1.3 Cold elastic collisions

Classically, the angular momentum of a particle approaching on a straight line a fixed target is $L = mvb$ where m is the particle mass, v its speed and

b the impact parameter which is approximately the effective distance for a central potential. Let's assume the particle moves slowly towards the target (low collisional energy), as a result L will be relatively small.

In a quantum description, if $mvb/\hbar = kb \ll 1$ that is $b \ll \lambda_{dB}$ where λ_{dB} is the de Broglie wavelength then we have $L/\hbar \ll 1$ that is $l \approx 0$. It means the particle does not have enough energy to pass the centrifugal barrier added to $U(r)$ since $k^2 \ll l(l+1)/b^2$. We can conclude that, for a cold (low energetic) collision, one can only consider the $l = 0$ term in 5.4 and 5.7. These kind of collisions are called s-wave collisions in relation to the spectroscopic notation for $l = 0$.

Let's have a look to what this approximation gives for important collision parameter such as f :

$$f(\theta) = \frac{\sin(\delta_0)}{k} e^{i\delta_0} \quad (5.8)$$

Using 5.3, the scattering cross section becomes:

$$\sigma_T = \int \left| \frac{\sin(\delta_0)}{k} e^{i\delta_0} \right|^2 d\Omega = 4\pi \frac{\sin^2(\delta_0)}{k^2} \quad (5.9)$$

Until now, the two colliding particles has been considered as distinguishable. Including the indistinguishable nature of a identical particles collision, it brings modifications to the expressions of wave functions, scattering amplitudes and cross sections. For bosons, the total wave function $\Psi(\mathbf{r})$ has to be symmetric in \mathbf{r} , for fermions it has to be anti-symmetric. Thus for a elastic collision between two bosons:

$$\sigma(\theta) = |f(\theta) + f(\pi - \theta)|^2$$

and for a collision between two fermions:

$$\sigma(\theta) = |f(\theta) - f(\pi - \theta)|^2$$

Considering s-wave collisions for ^{85}Rb or ^{87}Rb , which are bosons, σ_T becomes:

$$\sigma_T = 8\pi \frac{\sin^2(\delta_0)}{k^2}$$

We can introduce a new quantity for s-wave collisions which is the scattering amplitude a given by:

$$a \underset{k \approx 0}{\approx} -\frac{\delta_0}{k}$$

It is possible to link it to the total scattering cross section:

$$\sigma_T = 8\pi a^2$$

The scattering amplitude is an interesting quantity, it is a measure of the potential effective range without making any assumption on the shape of the potential itself. Two completely different $V(r)$ with the same a will result in identical s-wave scattering properties. Furthermore its sign is relative to the type of interactions between atoms, if $a < 0$ they are attractive and if $a > 0$ they are repulsive.

5.1.4 Conclusion

According to 5.6 the effect of an elastic scattering is just a phase shift between each incoming and outgoing partial wave since $\sin(kr - l\frac{\pi}{2} + \delta_l) = \frac{1}{2i}(e^{i(kr - l\frac{\pi}{2} + \delta_l)} - e^{-i(kr - l\frac{\pi}{2} + \delta_l)})$, there is no change in amplitude. There are not any changes of any internal degree of freedom either (such as the spin for instance). Elastic collisions are "good" collisions in a sense that they only thermalize the atomic cloud and are not the cause of losses.

5.2 Inelastic collisions

These kind of collisions will result in an energy transfer from internal degrees of freedom towards kinetic energy resulting in losses and heating [7], [8]. Such scattering events can involve two or three particles. Some aspects of these "bad" collisions are presented below.

5.2.1 Spin exchange collisions

If two atoms in a different hyperfine level collide they can experience a change in their hyperfine state while conserving the total angular momentum and its projection along the z-axis. For instance two atoms in a $(F = 2, m_F = 1)$ interacting can leave in a $(F = 2, m_F = 0)$ and a $(F = 2, m_F = 2)$ set but for two atoms initially in a $(F = 2, m_F = -2)$ state this interaction is not happening since a $(F = 2, m_F = -3)$ state does not exist. In a magnetic trap, such a hyperfine change can lead the atom to be in an untrappable state, therefore leading to losses. Furthermore, because of the presence of a magnetic field, the Zeeman splitting can cause one atom to gain kinetic energy. If this atom is in a dipole trap and if the energy gained is greater than the trap depth, the atom will leave the trap.

5.2.2 Magnetic dipole relaxation

This happens when the magnetic dipoles of the colliding atoms interact (atoms have a magnetic dipole created by the nucleus and the electron spin). Because of the nature of this interaction two s-waves colliding may leave in a d-wave channel [8]. As a consequence of the change in orbital momentum, there will be a change in hyperfine states to keep the projection along the z-axis of the total momentum F constant.

5.2.3 Three bodies molecular recombination

Molecule creation as a three-body process: two atoms bond together and the third one receive the binding energy thus resulting in heating or loss depending of the trap depth. This energy gain can be lowered if the collision energy is close to the binding energy, this is the case when a Feshbach resonance happens. These effect will be discuss in the next chapter.

Chapter 6

Feshbach resonances

6.1 Introducing Feshbach resonances

A Feshbach resonance happens when the collision energy is tuned into degeneracy with a bound state energy. This means that, with the help of an external field, one can dramatically increase the interactions between atoms or, identically, increase the rates of elastic and inelastic collisions [10]. It means that near a resonance, $|a|$ will significantly increase. Using a magnetic field to approach a Feshbach resonance, a has the form

$$a = a_0 \left(1 - \frac{\Delta}{B - B_0} \right)$$

where a_0 is the off-resonance scattering length B_0 is the field value at a resonance and Δ the resonance width. When B is swept through the resonance, a varies from highly negative to highly positive values changing the nature of the interaction from attractive to positive which is, for instance, an interesting feature for the study of BEC. ^{85}Rb and ^{87}Rb have Feshbach resonances. The resonance at $B = 155\text{G}$ for ^{85}Rb in the $(F = 2, m_F = -2)$ channel has been studied by many groups because it is a very pronounced resonance and its width is very large ($\approx 5\text{G}$). This is the resonance which will be studied here too.

The QDG group is very interested in using Feshbach resonances to study collision between Rb and Li and create heteronuclear molecules from these atoms and study their interactions.

6.2 Trap life time applying an homogeneous magnetic field

^{85}Rb was loaded in a MOT and then transferred in the IPG dipole trap, some MOT coils were used to create a homogeneous magnetic field (Helmholtz configuration). This field was swept in amplitude from 0 A to 12 A current in the coils and for each current the trap hold time was varied from 100 ms to 2 s (200 ms has to be added). Benjamin Deh's magnetic field calibration gives the magnetic field B as a function of the current I :

$$B = 31.8I$$

Thus 155 G Feshbach resonance happens for a current $I \approx 5\text{A}$. For this first measurement, 1 A steps were used between two data points so it was impossible to see the 5G wide Feshbach resonance. Typical trap losses with increased trap hold time are shown fig. 6.1. Losses happens because of inelastic collisions and background atoms collisions.

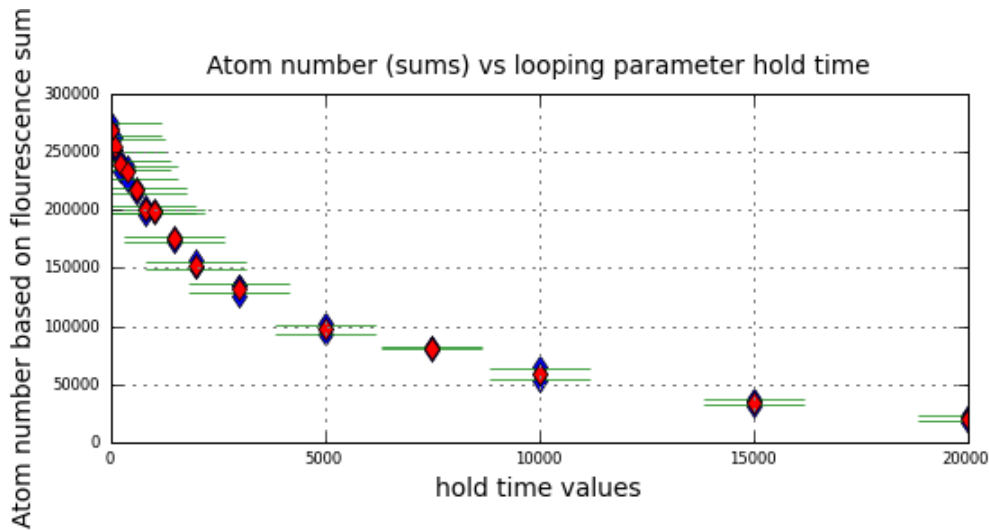


Figure 6.1: Atom losses while increasing trap hold time - $I = 2\text{ A}$

Each data curve was fitted by $f_1e^{-t/f^2} + f_3e^{-t/f^4}$, fig. 6.2 show the time constants versus magnetic field and fig. 6.3 show the fit exponentials amplitudes versus magnetic field. One decaying exponential was not enough to fit because of multiple sources of inelastic collisions.

One can see that the trap life time was decreasing when the magnetic field was increased. This means that either the field is not perfectly homogeneous so that Zeeman splitting at high field causes losses from inelastic

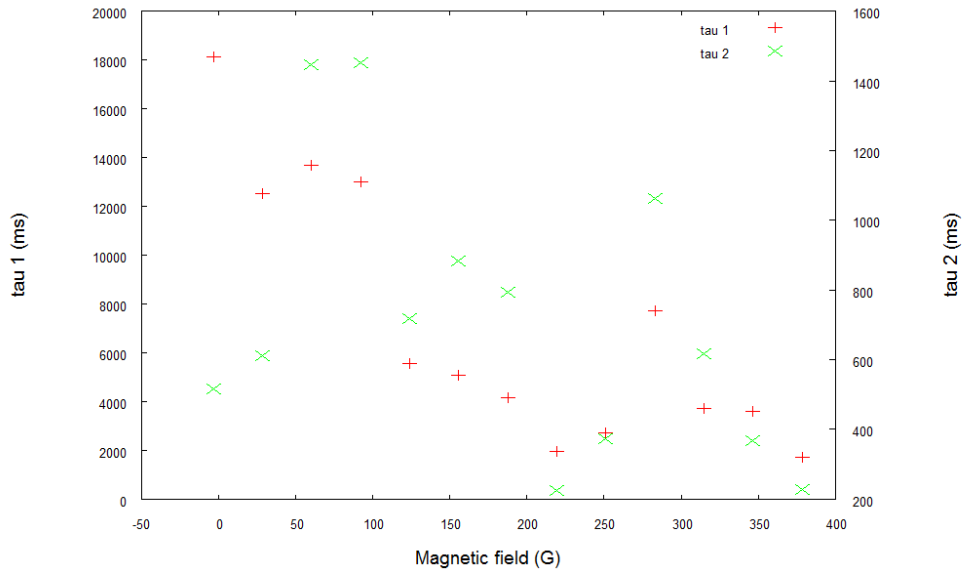


Figure 6.2: Trap life time

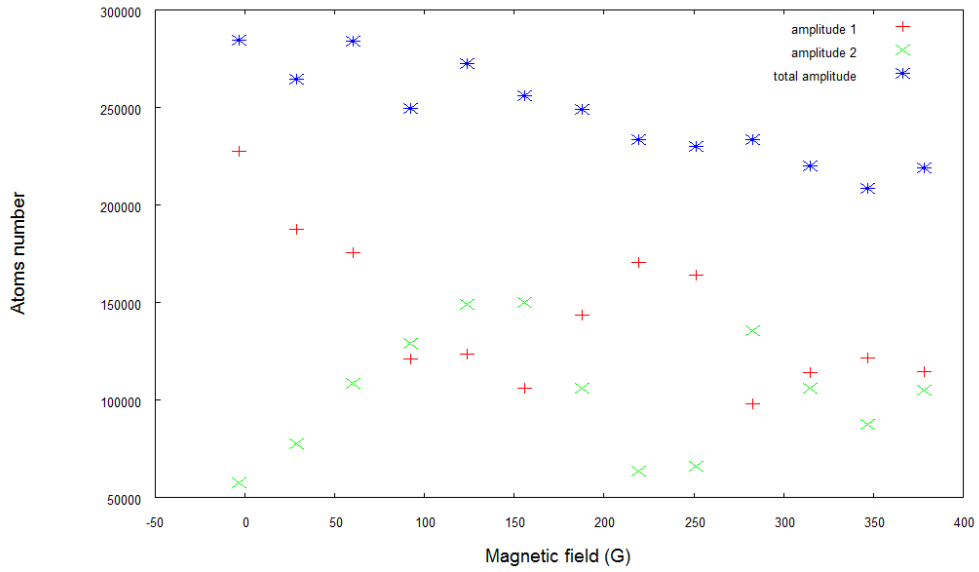


Figure 6.3: Fit amplitudes

collisions or the magnetic field is not homogeneous for some currents: it has been reported that oscillations in the coils driver could happen for some current values. The main information obtained from this measurement is that even when losses are maximum, trap life times are never below 2 s. So we can use the system to search for Feshbach resonances.

Comparing the dipole trap depth and the maximum energy gain because of a Zeeman state changing inelastic collision has been possible thanks to a James Booth python program modified by Bruce Klappauf. This code calculates eigenvalues (and eigenvectors) of the sum of the hyperfine structure and the hyperfine Zeeman hamiltonians. Using the code for ^{85}Rb it gives the curves shown in fig. 6.4. They are very similar to these from ref [2].

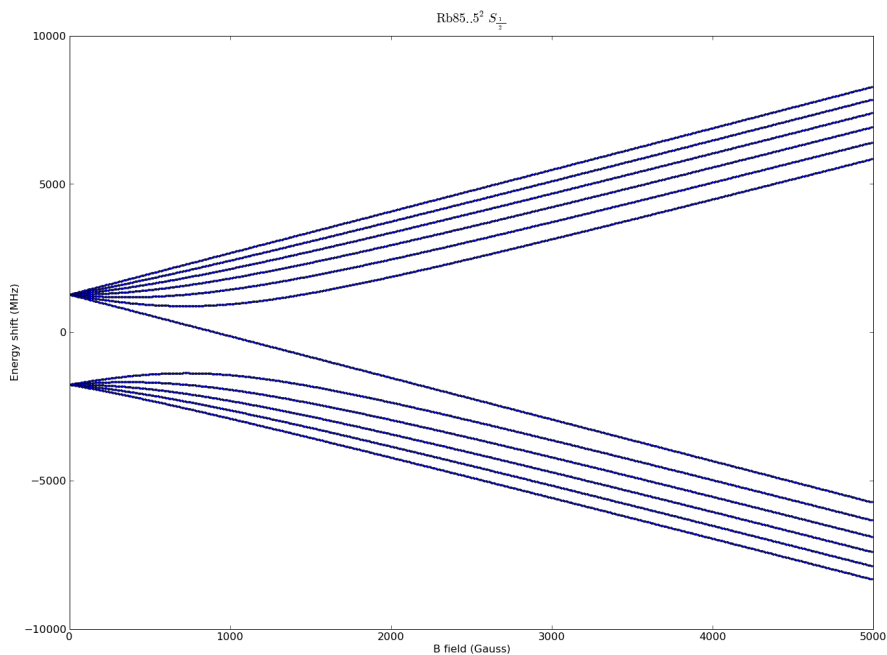


Figure 6.4: Eigenenergies versus magnetic field

If two atoms collide and leave in a different Zeeman sub-state the energy available in the center-of-mass frame from this internal state change will be :

$$E_{cm} = (E_{atom1} + E_{atom2})_{before\ collision} - (E_{atom1} + E_{atom2})_{after\ collision}$$

The energy E_{cm} will be transferred to kinetic energy and if it is greater than the trap depth the atom will very likely be lost. The energy lost $-E_{cm}$ as a function of magnetic field is shown fig. 6.5. According to Will Gunton's data, the depth is about $813\mu\text{K} \approx 16.9\text{ MHz}$ so trap losses will happen from a field of about 190 G.

This alone does not explain the drop of life time for small magnetic fields ($< 200\text{ G}$).

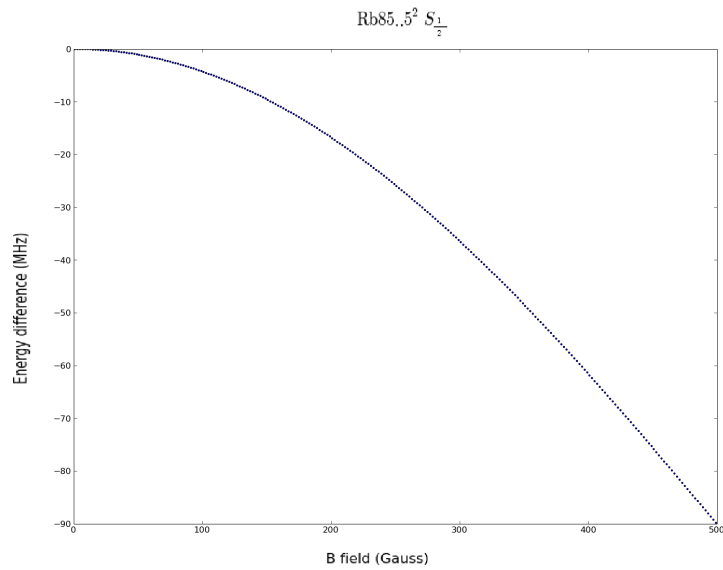


Figure 6.5: Energy lost in the collision because of Zeeman sub-state changing

6.3 Searching for Feshbach resonances

After measuring the trap life time, Feshbach resonances were searched even if the atoms are not all in the ($F = 2, m_F = -2$) state. The first try was with one second hold time in the dipole trap (see fig. 6.6).

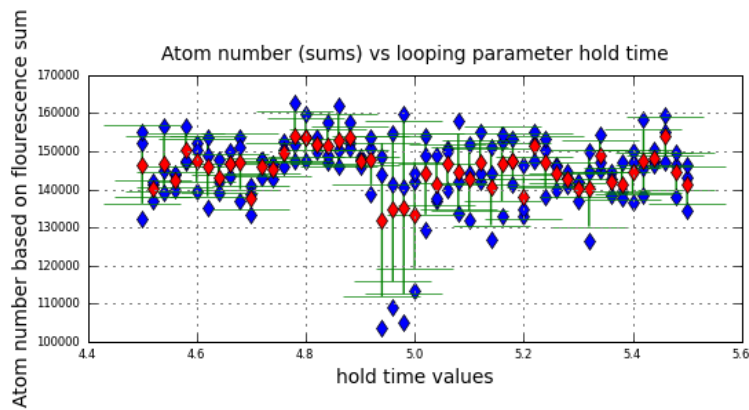


Figure 6.6: A Feshbach resonance ?

This drop may be a sign of a Feshbach resonance, the magnetic field is close to 155 G trusting the calibration of B. Deh. This and the width are consistent, so another run was made within a smaller current range, see fig. 6.7

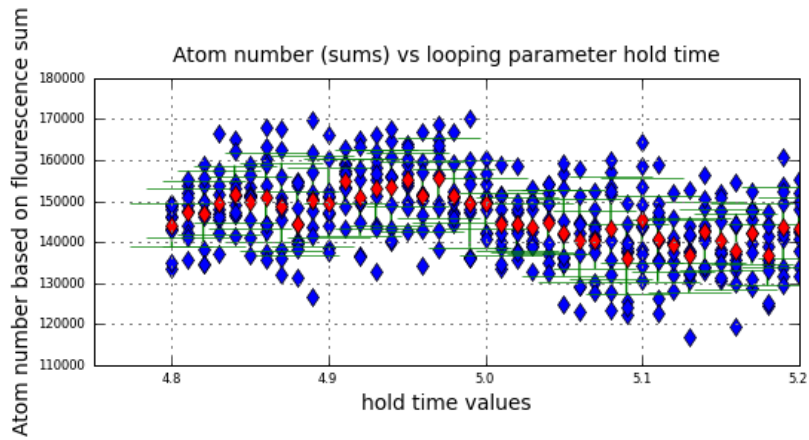


Figure 6.7: Disappearance of the "resonance"

As you can see the "resonance" seemed to have disappeared. This may be due to the mixing of Zeeman sub-states, other measurements were made after fixing this. For the new ones, the changing parameter is not the trap hold time but the time of exposure to the magnetic field. Results for different magnetic hold times are presented figures 6.8, 6.10 and 6.11.

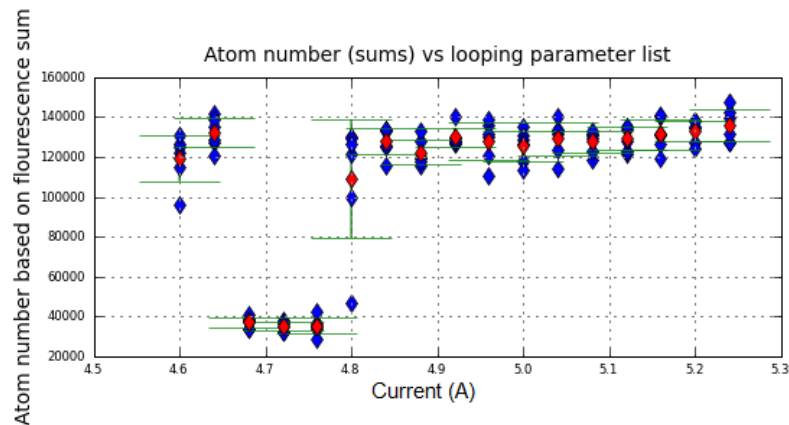


Figure 6.8: A Feshbach resonance ? - 1 s magnetic hold time

The resonance and its width seems to vary for each run, both variation would be explained by a variation of the magnetic field. Further investigation may include a verification of the coil driver, trying shorter magnetic hold times to see if the drop stop "saturating" to ≈ 40000 atoms and verify if the MOT is really recapturing when the "resonances" happen.

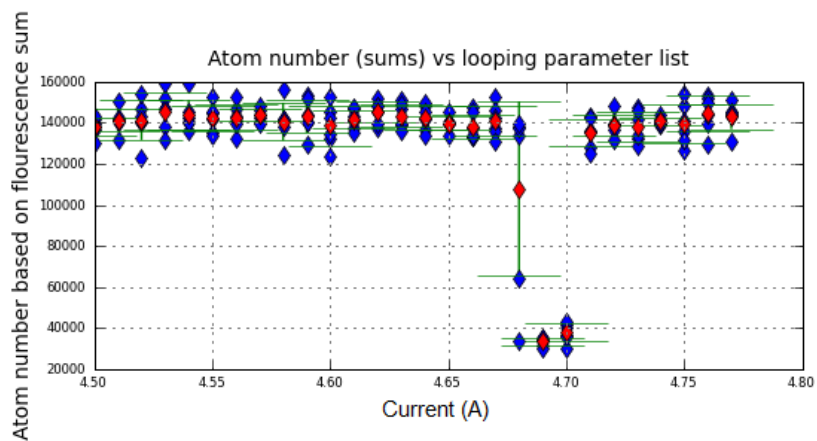


Figure 6.9: A Feshbach resonance ? - 1 s magnetic hold time - smaller range

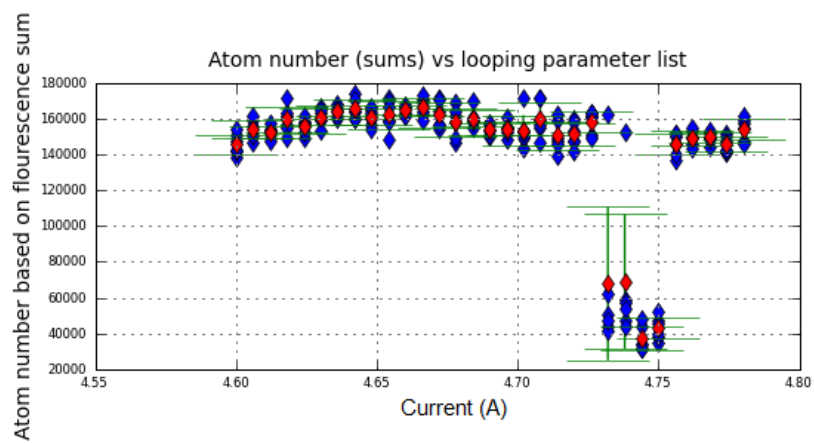


Figure 6.10: A Feshbach resonance ? - 500 ms magnetic hold time

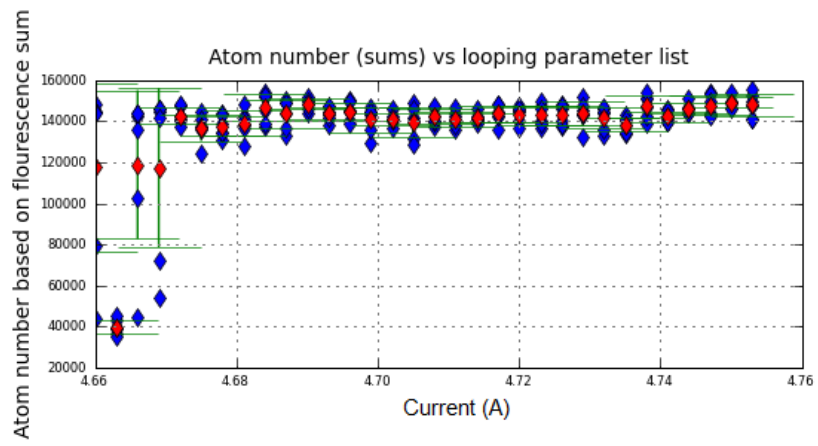


Figure 6.11: A Feshbach resonance ? - 250 ms magnetic hold time

Bibliography

- [1] A. Robinson, Measuring the Molecular Structure of Ultracold Lithium-Rubidium Dimers by Feshbach Resonances, Master thesis, University of British Columbia, 2009.
- [2] D. A. Steck, Rubidium 85 D Line Data and Rubidium 87 D Line Data, <http://george.ph.utexas.edu/~dsteck/alkalidata/>, 2008.
- [3] F. M. Gardner, *Phaselock Techniques* 3rd ed. , Wiley-Interscience, 2005.
- [4] J. D. Kraus, *Antennas* 2nd ed. , McGraw-Hill, 1988.
- [5] M. S. Child, *Molecular collision theory*, Dover Publications, 1996.
- [6] C. Cohen-Tannoudji, Condensation de Bose-Einstein des gaz atomiques ultra froids : effets des interactions, <http://www.phys.ens.fr/cours/college-de-france/>, 1999.
- [7] J. L. Roberts, Bose-Einstein Condensates with Tunable Atom-atom Interactions: The First Experiments with ^{85}Rb BECs, Ph.D. thesis, University of Colorado, 2001.
- [8] J. P. Burke, Theoretical Investigation of Cold Alkali Atom Collisions, Ph.D. thesis, University of Colorado, 1999.
- [9] S. L. Cornish, N. R. Claussen, J. L. Roberts, E.A. Cornell and C. E. Wieman, Stable ^{85}Rb Bose-Einstein Condensates with Widely Tunable Interactions, *Phys. Rev. Lett.* **85**, 1795 (2000)
- [10] J. L. Roberts, N. R. Claussen, S. L. Cornish, and C. E. Wieman Magnetic Field Dependence of Ultracold Inelastic Collisions near a Feshbach Resonance, *Phys. Rev. Lett.* **85**, 728 (2000)